# BARYCENTRIC NEURAL NETWORKS AND LENGTH-WEIGHTED PERSISTENT ENTROPY LOSS: A GREEN GEOMETRIC AND TOPOLOGICAL FRAMEWORK FOR FUNCTION APPROXIMATION

**Victor Toscano-Duran**,* **Rocio Gonzalez-Diaz**
Department of Applied Mathematics I, University of Seville
Seville, Spain
{vtoscano, rogodi}us.es

**Miguel A. Gutiérrez-Naranjo**
Department of Computer Science and Artificial Intelligence, University of Seville
Seville, Spain
magutier@us.es

**ABSTRACT**

While it is well-established that artificial neural networks are *universal approximators* for continuous functions on compact domains, many modern approaches rely on deep or overparameterized architectures that incur high computational costs. In this paper, a new type of *small shallow* neural network, called the *Barycentric Neural Network* (BNN), is proposed, which leverages a fixed set of *base points* and their *barycentric coordinates* to define both its structure and its parameters. We demonstrate that our BNN enables the exact representation of *continuous piecewise linear functions* (CPLFs), ensuring strict continuity across segments. Since any continuous function over a compact domain can be approximated arbitrarily well by CPLFs, the BNN naturally emerges as a flexible and interpretable tool for *function approximation*. Beyond the use of this representation, the main contribution of the paper is the introduction of a new variant of *persistent entropy*, a topological feature that is stable and scale invariant, called the *length-weighted persistent entropy* (LWPE), which is weighted by the lifetime of topological features. Our framework, which combines the BNN with a loss function based on our LWPE, aims to provide flexible and geometrically interpretable approximations of nonlinear continuous functions in resource-constrained settings, such as those with limited base points for BNN design and few training epochs. Instead of optimizing internal weights, our approach directly *optimizes the base points that define the* BNN. Experimental results show that our approach achieves *superior and faster approximation performance* compared to classical loss functions such as MSE, RMSE, MAE, and log-cosh. This efficiency aligns with the principles of *Green AI*, offering an effective trade-off between approximation performance and resource consumption. By unifying tools from geometry and topology within the neural network paradigm, our work provides a mathematically grounded yet computationally *sustainable framework for function approximation*.

***K*eywords** Barycentric Coordinates · Neural Networks · Persistent Entropy · Function Approximation · Green AI

## 1 Introduction

*Function representation and approximation* are fundamental problems in Machine Learning and scientific computing, underpinning a wide range of applications such as physical simulation, data modeling, and predictive analysis. A foundational result in this area is the *Universal Approximation Theorem*, which established that *artificial neural networks* (ANNs) are universal approximators, capable of approximating any continuous function over compact domains [15]. The theoretical study of ANNs as universal approximators has since evolved significantly, with further work demonstrating their capacity to approximate continuous and smooth functions effectively [10, 31, 16, 27]. More recent research

*Corresponding author.

has explored optimal approximation properties of sparsely connected deep networks [2] and the expressive power of ReLU-based architectures for function approximation [18, 23]. Although deep neural networks (DNNs) are powerful and are indeed known to be universal approximators, they typically require highly overparameterized architectures, large datasets, and significant computational resources for training. This often results in architectures (models) that are opaque, costly and energy-intensive. Such limitations are particularly problematic in settings with *limited* resources, such as embedded systems and edge computing, where lightweight and interpretable models are preferable.

The growing tension between performance and interpretability has motivated the development of more structured, explainable, and computationally efficient models. This aligns with the emerging paradigm of Green Artificial Intelligence (Green AI) [3], which advocates for energy-efficient and sustainable machine learning systems. In this context, *geometric and topological* tools have gained increasing attention for their ability to structure information and capture global patterns that go beyond local pointwise accuracy. On the geometric side, *barycentric coordinates* offer a classical yet underutilized approach for function approximation. These coordinates allow points to be expressed as convex combinations of the vertices of a simplex, enabling a natural mechanism for piecewise linear interpolation. Historically applied in computer graphics and geometric design [30], barycentric interpolation has recently been extended to function approximation [22]. While [22] employs barycentric subdivisions, which lead to an exponential growth in the size of the triangulations, our approach does not rely on such subdivisions. These approaches demonstrate that fixed geometric structures can yield accurate and efficient representations, especially for continuous piecewise linear functions. Nested barycentric coordinate systems (NBCS) have been proposed to represent complex function spaces in a composable and interpretable manner [12]. Similarly, variational barycentric interpolation has been explored for mesh-based learning and shape optimization [7]. Despite their potential, geometric techniques, like barycentric coordinates, are rarely integrated into trainable models for function approximation, despite remaining decoupled from neural network architectures.

On the topological side, topological methods have also been integrated into analysis and machine learning. *Persistent homology*, a core method in *topological data analysis* (TDA), and its associated summaries, like *persistent entropy*, have proven valuable for extracting global, deformation-invariant features from data. Initially used for feature extraction, TDA provides stable and noise-robust descriptors based on the birth and death of topological features such as connected components, loops, and voids, that can be used as input data for machine learning models across diverse tasks, such as characterizing idiotypic immune networks [25], analyzing similarities in piecewise linear functions and time series [26], and defining safety regions for robotic navigation [29]. More recently, the field of *Topological Deep Learning* (TDL) has emerged, incorporating persistent homology into the training of neural networks through differentiable topological layers and loss functions [33]. For instance, persistent homology and associated descriptors have been used to inject shape-aware constraints into neural networks, yielding improvements in tasks like anatomical segmentation [19], point cloud reconstruction [14], shape classification [24], and time series forecasting [17]. Recent advances in differentiable topological optimization [4, 32] have further improved the trainability and robustness of topological loss functions, making them viable components for neural network training pipelines. These topological losses aim to preserve global structural properties in learned functions, which classical loss functions like MSE tend to overlook. However, challenges persist, including gradient sparsity and computational inefficiency, which have limited their use in practice.

In this paper, we propose a *novel, interpretable, and sustainable framework that combines geometric and topological methods for function approximation*. We first introduce a new type of shallow neural network, the so-called *Barycentric Neural Network* (BNN). Such neural network architecture enables efficient piecewise linear interpolation, making it well-suited for representing Continuous Piecewise Linear Functions (CPLFs), ensuring strict continuity across segments. Since any continuous function over a compact domain can be approximated arbitrarily well by CPLFs, the BNN naturally emerges as a flexible, interpretable, and resource-efficient tool for function approximation. We use barycentric coordinates to define the internal parameters of the proposed neural network architecture. This way, the BNN is fully determined by a set of trainable *base points and their corresponding barycentric coordinates*. These base points serve as the vertices of the simplices over which barycentric interpolation is performed. As a result, unlike traditional neural networks that require tuning internal weights through backpropagation, training a BNN reduces *to optimizing the base points* while the network's parameters remain fixed by construction and depend exclusively on these base points. The number of base points can be specified in advance by the user and directly determines both the size and the expressiveness of the architecture: the larger the set, the more complex the architecture becomes and the greater its approximation capacity.

Our goal is to approximate a target continuous function, assuming we have limited resources, as only a small set of such base points and a few training epochs, based on the intuition that the more representative these points are, the better the approximation. To further improve approximation quality, we introduce a novel loss function based on a new topological summary statistic that we define, called *length-weighted persistent entropy* (LWPE). This statistic is a modified version of classical persistent entropy [5], a stable and scale-invariant topological descriptor, enriched by weighting the contribution of each topological feature by its lifespan (i.e., persistence). We then employ this

LWPE-based loss function in our framework, guiding the optimization of the BNN's base points through topological information. Unlike classical loss functions such as MSE, RMSE, MAE, or log-cosh, this approach preserves not only pointwise accuracy but also the global topological structure of the target function. By combining the BNN with the LWPE-based loss, our framework achieves superior function approximation compared to traditional loss functions when a limited number of base points and training epochs are used, aligning our methodology with the goals of Green AI. This is particularly useful in applications where topology carries semantic meaning, such as preserving peaks and valleys in economic indicators, motifs in biological signals, or capturing global trends in physical models.

The key contributions of this work are as follows:

- **Barycentric Neural Network:** We propose a scalable and shallow neural network, the so-called *Barycentric Neural Network*, for representing continuous piecewise linear functions. Its structure and parameters are fixed, based on a predefined set of points, called *base points*, and their barycentric coordinates.
- **Optimization on the base points:** Instead of relying on backpropagation for weight tuning, the BNN's training is entirely based on optimizing the positions of its base points, yielding a geometrically and more efficient training process.
- **Topological loss function:** We propose a novel topological summary statistic, the length-weighted persistent entropy (LWPE), which serves as the basis for a new loss function. This formulation provides a topologically informed mechanism that enhances both convergence and the quality of function approximation using BNNs with a limited number of base points.
- **Experimental validation:** We empirically validate the effectiveness of our approach (BNN trained with our LWPE-based loss function) for function approximation using both synthetic and real-world data, showing superior performance and efficiency compared to using classical loss functions (e.g., MSE, RMSE, MAE and log-cosh), under resource-constrained settings, such as limited base points for BNN design and few training epochs.

By integrating geometric and topological tools into neural network design, this work bridges theoretical advances with practical utility, contributing to the ongoing development of efficient, interpretable and sustainable Machine Learning methodologies, while also enriching the emerging field of geometric and topological deep learning. In particular, it offers a practical alternative to traditional overparameterized deep networks in scenarios that demand structural guarantees and computational efficiency, such as function approximation under limited resources.

The remainder of this paper is organized as follows: Section 2 introduces the preliminary notions related to the different topics involved in the paper, such as barycentric coordinates, persistent homology and persistent entropy. Section 3 introduces our proposed variant of persistent entropy, the length-weighted persistent entropy. Section 4 details how barycentric neural networks are defined. In Section 5, we present the experiments conducted, including an explanation of how our length-weighted persistent entropy-based loss function is defined, and how we use it for function approximation in combination with the barycentric neural network, along with the results obtained. Finally, conclusions, limitations and future work are given in Section 6.

## 2 Preliminaries

This section introduces the main concepts and establishes some notations that are used throughout the paper. We begin by introducing CPLF, followed by the key concepts of computational topology employed in this work, including simplicial complexes, barycentric coordinates, persistent homology, and persistent entropy. A general introduction to computational topology can be found, for example, in [8, 21].

### Continuous Piecewise Linear Functions

Fixed $d \in \mathbb{N}$, a *Continuous Piecewise Linear Function* (CPLF) is a function $h : C \subseteq \mathbb{R}^d \to \mathbb{R}$, where the domain $C$ is the union of specific regions $|\sigma_0|, \ldots, |\sigma_n|$ (called $d$-simplices, defined later). On each simplex $|\sigma_k|$, the function $h$ is given by a linear expression: $h(p) = m_k \cdot p + c_k$, for some $m_k \in \mathbb{R}^d$. $c_k \in \mathbb{R}$, and $p \in |\sigma_k|$. Importantly, the function $h$ is required to be globally continuous, ensuring that the linear expressions agree on overlapping regions, that is, $m_i \cdot p + c_i = m_j \cdot p + c_j$ whenever $p \in |\sigma_i| \cap |\sigma_j|$.

Finally, given any continuous function $f\colon \mathbb{R}^d \to \mathbb{R}$, a CPLF $h\colon C \subset \mathbb{R}^d \to \mathbb{R}$ approximates $f$ on $C$ with approximation error given by:

$$||f - h|| = \max\left\{|f(p) - (m_k \cdot p + c_k)|\colon p \in C \cap |\sigma_k| \text{ and } k \in \{0, 1, \ldots, n\}\right\}.$$

**Remark 1.** *In this paper, only* CPLF *functions $h : [A, B] \subset \mathbb{R} \to \mathbb{R}$, where $[A, B]$ is the domain interval with endpoints $A, B \in \mathbb{R}$, will be considered for experiments in Section 5. In that case, for some $n \in \mathbb{N}$, the domain interval $[A, B]$ of $h$ is divided into $n + 1$ subintervals $[a_i, b_i]$, where $A = a_0 < b_0 = a_1 < \cdots < b_{n-1} = a_n < b_n = B$. The function $h$ is continuous at the joining points, that is, $m_{i-1} \cdot b_{i-1} + c_{i-1} = m_i \cdot a_i + c_i$. Any given continuous function $f : [A, B] \subset \mathbb{R} \to \mathbb{R}$ can be approximated as closely as desired by a* CPLF *$h : [A, B] \to \mathbb{R}$ by partitioning $[A, B]$ into a a sufficiently large finite number of segments.*

### Simplicial Complexes

Any compact subset $\mathcal{C}$ of $\mathbb{R}^d$ can be approximated by a simplicial complex (see, for example, [20, Chapter 1]). The combinatorial structure of such complexes allows for efficient computation of topological information using discrete algorithms. Given $d \in \mathbb{N}$, a *(finite, $d$-dimensional, embedded in $\mathbb{R}^d$) simplicial complex* $\mathcal{K}$ consists of:

- A finite set of points $V \subset \mathbb{R}^d$ called vertices or 0-simplices,
- For $k \in \{1, 2, \ldots, d\}$, a finite set of $k$-simplices. Any $k$-simplex $\sigma$ of $\mathcal{K}$ is the convex hull of $k + 1$ affinely independent vertices $\{v_0, \ldots, v_k\} \subset V$ (i.e., in general position). By abuse of notation, we write $|\sigma|$ to express the convex hull of the vertices of $\sigma$ and $\sigma = \{v_0, \ldots, v_k\}$ to detail its vertices.
- Any $k$-simplex $\sigma \in \mathcal{K}$ has $k + 1$ faces. Each face is the $(k + 1)$-simplex obtained by removing one vertex of $\sigma$.
- If $\sigma \in \mathcal{K}$, all faces of $\sigma$ also belongs to $\mathcal{K}$.
- The non-empty intersection of two simplices of $\mathcal{K}$ is a face of both.

### Barycentric Coordinates

Barycentric coordinates naturally connect geometry to topology through simplicial complexes. In any dimension $d$, barycentric coordinates $(t_0, t_1, \ldots, t_d)$ describe the location (position) of a point $p \in \mathbb{R}^d$ within the vertices of a $d$-simplex. Formally, for any simplex $\sigma = \{v_0, v_1, \ldots, v_d\}$ with vertices $v_i \in \mathbb{R}^d$ in general position and any point $p \in |\sigma| \subset \mathbb{R}^d$, there exists unique real values $(t_0, t_1, \ldots, t_d)$ such that:

$$p = \sum_{i=0}^{d} t_i v_i, \quad \text{with } t_i \geq 0 \text{ and } \textstyle\sum_{i=0}^{d} t_i = 1.$$

This representation allows a continuous interpolation across the simplices of a simplicial complex.

The barycentric coordinates of a point $p = (p_1, \ldots, p_d)^T \in \mathbb{R}^d$ with respect to a simplex $\sigma = \{v_0, v_1, \ldots, v_d\}$ can always be computed. If we write the coordinates of the point $p$ and the vertices $v_i$ in column form, then we have:

$$\begin{pmatrix} t_0 & t_1 & \cdots & t_d \end{pmatrix}^T = \begin{pmatrix} v_0 & v_1 & \cdots & v_d \\ 1 & 1 & \cdots & 1 \end{pmatrix}^{-1} \cdot \begin{pmatrix} p \\ 1 \end{pmatrix}.$$

This formulation ensures that $\sum_{i=0}^{d} t_i = 1$ and that $t_i \geq 0$ for all $i \in \{0, 1, \ldots, d\}$ if and only if $p$ lies in $|\sigma|$. Besides, the inverse of the $(d+1) \times (d+1)$-matrix $\begin{pmatrix} v_0 & v_1 & \cdots & v_d \\ 1 & 1 & \cdots & 1 \end{pmatrix}$ always exists because $\{v_0, v_1, \ldots, v_d\}$ are in general position.

**Remark 2.** *The barycentric coordinates of a point $x \in \mathbb{R}$ with respect to an interval (i.e., a 1-simplex) $[a, b] \subset \mathbb{R}$ are $(t, 1 - t)$ with $t = \frac{x-a}{b-a}$. Then, $(1 - t, t) \in [0, 1]^2$ if and only if $x \in [a, b]$.*

### Lower Star Filtration

Fixed $d \in \mathbb{N}$, let us consider a simplicial complex $\mathcal{K}$ with real values assigned to its vertices $V \subset \mathbb{R}^d$, denoted by $g \colon \mathbb{R}^d \to \mathbb{R}$. The *lower star* of a vertex $u \in V$ is the subcomplex that consists of all the simplices $\sigma$ of $\mathcal{K}$ such that $u$ is the minimum vertex of $\sigma$, that is $u \in \sigma$ and $g(u) \leq g(v)$ for any $v \in \sigma$. Assuming $V$ is composed by vertices $\{u_0, u_1, \ldots, u_m\}$ with distinct values $g(u_0) < g(u_1) < \ldots < g(u_m)$, the *lower star filtration of* $\mathcal{K}$ is the increasing sequence of simplicial complexes $\mathcal{K}(1) \subset \mathcal{K}(2) \subset \cdots \subset \mathcal{K}(n) = \mathcal{K}$ where $\mathcal{K}(i)$ is the lower star of vertex $u_i$. See [8, Chapter VI]. As we will see later, this filtration will be used to compute homology, and consequently persistent entropy, as well as our topological loss function, which guides the optimization of the base points in BNNs.

**Persistent Homology, Persistence Diagrams and Barcodes**

Persistent homology is a tool for studying data geometry and connectivity across scales. Using this tool and given a *filtered simplicial complex* (e.g., lower star filtration), one can effectively compute $q$-dimensional topological features at different scales, tracking features as they appear (birth) and disappear (death). Persistence diagrams and barcodes are visual representations used in the study of persistent homology and represent the birth and death (end) of topological features across scales. A $q$-dimensional persistence diagram plots points $(b, e)$ corresponding to the lifespans of $q$-dimensional topological features, while a barcode represents them as a *bar* starting at $b$ and ending at $e$. Specifically, a $q$-dimensional persistence diagram $D = \{(b_i, e_i) \mid i \in I\}$ satisfies that $b_i \leq e_i$ for all $i \in I$, and $I$ is the index set that identifies the pairs $(b_i, e_i)$ in $D$. Each pair $(b_i, e_i)$ corresponds to a $q$-dimensional topological feature that *appears* at time $b_i$ (birth) and *disappears* at time $e_i$ (death, i.e., end) as the filtration progresses. Both persistence diagrams and barcodes facilitate the understanding of feature persistence in data. Fig. 1 shows a persistence diagram (center) alongside its corresponding barcode (right), illustrating the persistence of topological features in the data.

The number of bars of the barcode associated with the lower star filtration of a simplicial complex $\mathcal{K}$ is less than or equal to half of the number of vertices of the simplicial complex $\mathcal{K}$ plus 1. Given the lower star filtration on a simplicial complex $\mathcal{K}$ with vertex set $V$, local critical points are always located at the vertices of $V$ and can be effectively computed from the *lower link* of each vertex $v$ of $V$, which consists of the simplices of $\mathcal{K}$ in the closed lower star that do not belong to the lower star of $v$. We call $v$ a local critical vertex of index $q$ if its lower link has the reduced homology of the $(q-1)$-sphere. Then, $q$-dimensional persistence diagrams pair critical vertices of index $q$ (when topological features are born) with critical vertices of index $q+1$ (when topological features die). A detailed description can be found in [9, Chapter VI].

**Remark 3.** *In the case of 0-dimensional persistent homology (the one considered in the experiments of this paper), the number of topological features (number of points in persistent diagram, and number of bars in persistent barcode) is tight: with $2n-1$ vertices, one can obtain a 0-dimensional barcode with $n$ bars since local minima (vertices where connected components are born) are paired with local maxima (vertices where connected components die) through the 0-dimensional persistence diagrams and barcodes. By convention, we truncate the death of the oldest connected component to $\max f$. This way, when we use the lower-star filtration, the longest bar is always $[\min f, \max f)$. Figure 1 illustrates this with a simplicial complex composed of vertices (points) and edges (union between points) whose function $f$ is derived from the sine function, producing four local minima paired with maxima, represented by four bars. This way, we can obtain the same barcode, just with seven vertices (being four local minima and three local maxima).*

**Persistent entropy**

Persistent entropy (PE) [5] *measures* the complexity of a topological space based on its persistence diagram $D = \{(b_i, e_i) \mid i \in I\}$. It is defined as :

$$\mathrm{PE} = -\sum_{i \in I} p_i \ln p_i, \qquad \text{where } p_i = \tfrac{\ell_i}{L}, \text{ being } \ell_i = e_i - b_i \text{ and } L = \textstyle\sum_{i \in I} \ell_i. \tag{1}$$

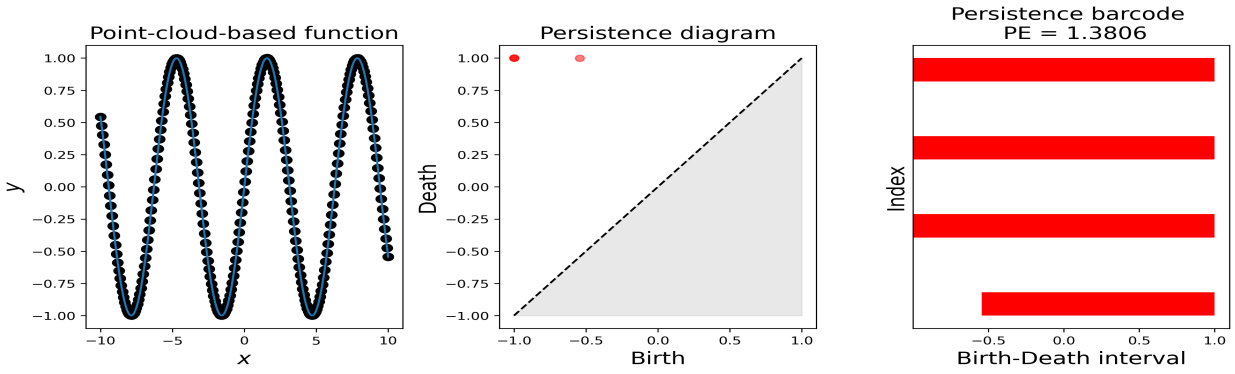


Figure 1: The figure shows a simplicial complex with 250 vertices (point-cloud-based function with 250 points) representing the sine function (left), its persistence diagram (middle), barcode, and persistent entropy (right), all from the lower-star filtration.

Persistent entropy reflects the uniformity of bar lengths in a persistence barcode. Its maximum is attained when all bars have equal length, in which case it is given by $\mathrm{PE} = \ln(\#I)$, where $\#I$ denotes the cardinality of $I$ (i.e., the number of

bars in the persistence diagram $D$). Conversely, its minimum value is $\mathrm{PE} = 0$, which occurs when the barcode contains a single long bar and the remaining bars have negligible length. Moreover, the greater the disparity among bar lengths, the closer the value of persistent entropy is to its minimum.

The stability results on persistence diagrams [6] and persistent entropy [1, 26] provide a robust foundation for quantifying the stability of topological features under small perturbations. Specifically, it is ensured that small changes in the input correspond to bars of short lengths in the persistence barcode and small, bounded changes in the persistent entropy. This property is particularly valuable in applications where small variations in data or model outputs, such as those encountered in numerical approximations or machine precision errors, might otherwise introduce significant uncertainties in analytical results. As an illustration, the persistent entropy computed in the example shown in Fig. 1 is 1.3806.

## 3 Lenght-Weighted Persistent Entropy

Computing persistent entropy using lower star filtration, is suitable for comparing discrete piecewise linear functions and analyzing time series data [25]. However, standard persistent entropy presents a fundamental limitation: two different functions can still share a similar persistent entropy, as the entropy only encodes a global distribution of bar lengths in the persistence diagram, not taking into account its length. To address this issue, we propose a new persistent entropy variant: the *length-weighted persistent entropy* (LWPE). Formally, we define LWPE as:

$$\mathrm{LWPE} = -\sum_{i \in I} \ell_i \ln p_i, \qquad \text{where } p_i = \tfrac{\ell_i}{L},\ \ell_i = e_i - b_i \text{ and } L = \textstyle\sum_{i \in I} \ell_i. \tag{2}$$

This formulation maintains the entropy structure but introduces a crucial weighting mechanism based on the length of the bars. While PE captures the uncertainty in bar distributions, LWPE incorporates the total bar lengths, giving more weight to longer, topologically significant features.

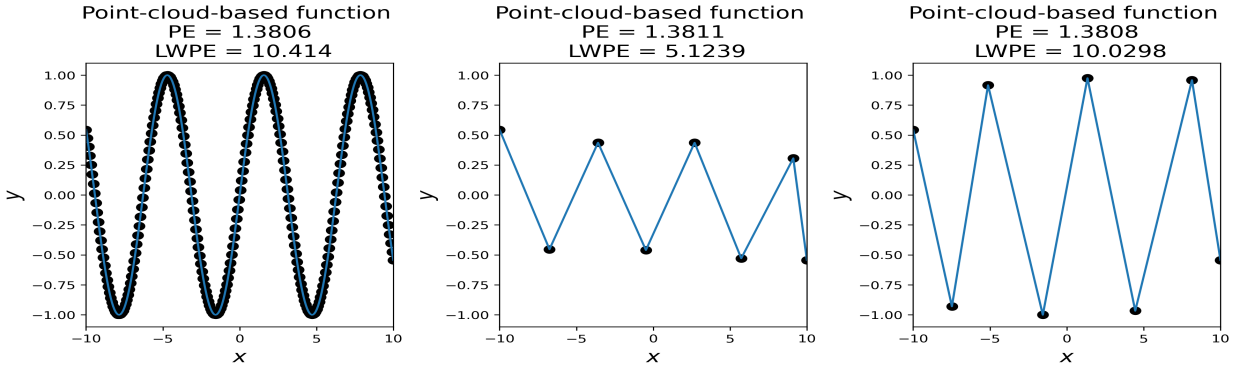


Figure 2: Comparison of persistent entropy (PE) and length-weighted persistent entropy (LWPE) on three subsampled versions of the sine function. The corresponding PE and LWPE values are reported in the title of each subplot.

Figure 2 illustrates standard persistent entropy limitation with three different subsampled versions of the same sine function. Although the point-cloud representations exhibit clear differences in resolution, the values of PE remain remarkably close. This occurs because PE primarily captures the global balance of bar lengths rather than their absolute scale. For instance, in the middle plot, the function is represented with very few points, but since the relative proportions of the peaks are preserved, the persistence diagram remains proportionally similar to that of the original function, resulting in a nearly identical PE value despite the drastic reduction in resolution. In contrast, as shown in the same plot, LWPE reveals that such a coarse representation is insufficient: it is not enough to preserve proportional bar lengths in the diagram, but rather a similar peak structure is also required to achieve comparable values. This is why the right plot, where both the proportions and the peaks are consistent with the original, yields LWPE values that are closer, while the middle plot does not. As we will see later in Section 5, using LWPE in our framework leads to significantly better approximation quality in practice than using classical persistent entropy.

## 4 Barycentric Neural Networks (BNNs)

Generally speaking, a *neural network* can be viewed as a parametrized mathematical function $N_\theta : \mathbb{R}^d \to \mathbb{R}^m$, where $\theta$ represents the set of parameters that define the network architecture. In an abuse of notation, such set of parameters

includes weights, bias, activation functions, and other architectural considerations like the number and type of layers. A general introduction to neural networks can be found in [13].

In this paper, we focus on one of the simplest types of artificial neural networks, the *multi-layer feed-forward networks*, which consist of sequences of stacked densely connected layers including input, hidden and output layers. The operation of a hidden layer can be mathematically expressed as: $y = h(Wx + b)$, where $x \in \mathbb{R}^d$ is the input vector, $W \in \mathbb{R}^{m\times d}$ is the weight matrix, $b \in \mathbb{R}^m$ is the bias vector, and $h$ is a nonlinear activation function (e.g., ReLU).

**Definition 1.** *Given a function $g : \mathbb{R}^d \to \mathbb{R}$ and a $d$-simplex $\sigma = \{v_0, \dots, v_d\}$ with vertices $v_i \in \mathbb{R}^d$, the barycentric neural network $\mathrm{BNN}_\sigma$ associated with $\sigma$ is defined as:*

$$\mathrm{BNN}_\sigma\left((t_0, t_1, \dots, t_d)\right) = \sum_{i=0}^{d} \mathrm{ReLU}\left(1 - \mathrm{ReLU}(1 - t_i) - \sum_{j=0}^{d}\left(\mathrm{step}^*(-t_j) + \mathrm{step}^*(t_j - 1)\right)\right) \cdot g(v_i)\,,$$

*where $(t_0, t_1, \dots, t_d)$ are the barycentric coordinates of a given $p \in \mathbb{R}^d$ with respect to $\sigma$, ReLU corresponds to the activation function defined by $\mathrm{ReLU}(t) = \max\{0, t\}$, for $t \in \mathbb{R}$, and $\mathrm{step}^*$ is the activation function defined as follows:*

$$\mathrm{step}^*(t) = 1 - \mathrm{step}(-t) = \begin{cases} 1 & \text{if } t > 0 \\ 0 & \text{if } t \leq 0, \end{cases}$$

*where $\mathrm{step}(t) = 1$ if $t \geq 0$ and 0 otherwise.*

**Lemma 1.** *Let $\sigma = (v_0, v_1, \dots, v_d)$ be a $d$-simplex with vertices $v_i \in \mathbb{R}^d$. Let $p \in \mathbb{R}^d$ with barycentric coordinates $(t_0, t_1, \dots, t_d)$ with respect to $\sigma$. We have:*

(a) *If $p \in |\sigma|$ then $\mathrm{BNN}_\sigma\left((t_0, t_1, \dots, t_d)\right) = \sum_{i=0}^{d} t_i \cdot g(v_i)$.*

(b) *If $p \notin |\sigma|$ then $\mathrm{BNN}_\sigma\left((t_0, t_1, \dots, t_d)\right) = 0$.*

*Proof.* Let us prove the statements.

(a) If $p \in |\sigma|$ then $t_i \in [0, 1]$ for all $i \in \{0, 1, \dots, d\}$ by definition of barycentric coordinates. Then $\mathrm{step}^*(-t_j) = 0 = \mathrm{step}^*(t_j - 1)$ for all $j \in \{0, 1, \dots, d\}$ and therefore,

$$\mathrm{ReLU}\left(1 - \mathrm{ReLU}(1 - t_i) - \sum_{j=0}^{d}\left(\mathrm{step}^*(-t_j) - \mathrm{step}^*(t_j - 1)\right)\right) = \mathrm{ReLU}\left(1 - \mathrm{ReLU}(1 - t_i)\right) = t_i.$$

We then have that $\mathrm{BNN}_\sigma\left((t_0, t_1, \dots, t_d)\right) = \sum_{i=0}^{d} t_i \cdot g(v_i)$.

(b) If $p \notin |\sigma|$ then, by the definition, the barycentric coordinates $(t_0, t_1, \dots, t_d)$ of $p$ with respect to $\sigma$ satisfy that there is a non-emtpy set $J \subset \{0, 1, \dots, d\}$ such that for any $j \in J$, $t_j < 0$ or $t_j > 1$. In that case, $\mathrm{step}^*(-t_j) = 1$ and $\mathrm{step}^*(1 - t_j) = 0$, or $\mathrm{step}^*(-t_j) = 0$ and $\mathrm{step}^*(t_j - 1) = 1$. Therefore, $\mathrm{step}^*(-t_j) + \mathrm{step}^*(t_j - 1) = 1$. Then,

$$\sum_{j=0}^{d}\left(\mathrm{step}^*(-t_j) + \mathrm{step}^*(t_j - 1)\right) \geq 1$$

and therefore,

$$\mathrm{ReLU}\left(1 - \mathrm{ReLU}(1 - t_i) - \sum_{j=0}^{d}\left(\mathrm{step}^*(-t_j) + \mathrm{step}^*(t_j - 1)\right)\right) = 0$$

for all $i \in \{0, 1, \dots, d\}$, concluding that $\mathrm{BNN}_\sigma\left((t_0, t_1, \dots, t_d)\right) = 0$.

□

**Remark 4.** *Consider the* $1D$ *case of a function* $g : \mathbb{R} \to \mathbb{R}$ *and a 1-simplex* $\sigma = \{a, b\}$ *with* $a < b \in \mathbb{R}$*. We have that the barycentric coordinates of a point* $x \in \mathbb{R}$ *with respect to* $\sigma$ *are* $(1-t, t)$*, being* $t = \frac{x-a}{b-a}$*. Then,*

$$\begin{aligned}
\mathrm{BNN}_\sigma\big((1-t,t)\big) &= \mathrm{ReLU}\big(1 - \mathrm{ReLU}(t) - (\mathrm{step}^*(t-1) + \mathrm{step}^*(-t) \ + \mathrm{step}^*(-t) + \mathrm{step}^*(t-1)\ )\big)\cdot g(a) \\
&\quad + \mathrm{ReLU}\big(1 - \mathrm{ReLU}(1-t) - (\mathrm{step}^*(t-1) + \mathrm{step}^*(-t) + \mathrm{step}^*(-t) + \mathrm{step}^*(t-1)\ )\big)\cdot g(b) \\
&= \mathrm{ReLU}\Big(1 - \mathrm{ReLU}(t) - 2\cdot(\mathrm{step}^*(t-1) + \mathrm{step}^*(-t))\Big)\cdot g(a) \\
&\quad + \mathrm{ReLU}\big(1 - \mathrm{ReLU}(1-t) - 2\cdot(\mathrm{step}^*(t-1) + \mathrm{step}^*(-t))\big)\cdot g(b) \\
&= \mathrm{ReLU}\big(1 - \mathrm{ReLU}(t) - 2\,\mathrm{step}^*(t-1) - 2\,\mathrm{step}^*(-t)\big)\cdot g(a) \\
&\quad + \mathrm{ReLU}\big(1 - \mathrm{ReLU}(1-t) - 2\,\mathrm{step}^*(t-1) - 2\,\mathrm{step}^*(-t)\big)\cdot g(b).
\end{aligned}$$

*Therefore,* $\mathrm{BNN}_\sigma\big((1-t,t)\big) = 0$ *if* $t < 0$ *or* $t > 1$*, that is, if* $x$ *is outside the closed interval* $[a, b]$*, ensuring locality.*

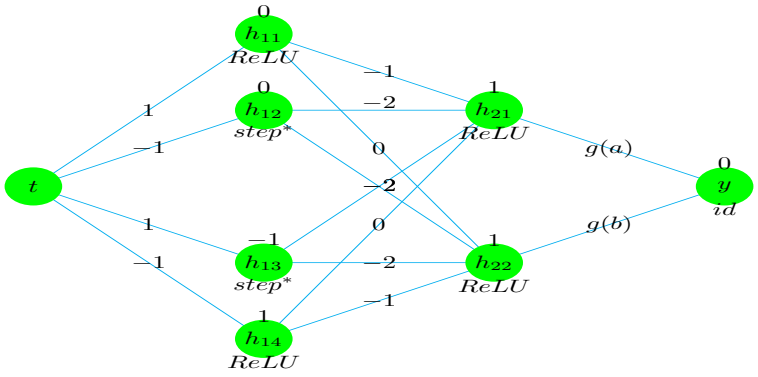


Figure 3: Structure and parameters of $\mathrm{BNN}_\sigma$ in the case of $\sigma = \{a, b\}$, with $a < b \in \mathbb{R}$. Each hidden neuron is denoted as $h_{ij}$, where $i$ indicates the hidden layer and $j$ the neuron index within that layer (e.g., $h_{22}$ is the second neuron of the second hidden layer). The numbers written above the neurons correspond to biases, while the labels below indicate the activation functions. The numbers on the edges represent weights.

As we can see in Fig. 3, in the case of $\sigma = \{a, b\}$ with $a < b \in \mathbb{R}$, $\mathrm{BNN}_\sigma$ corresponds to a multi-layer feedforward network with a single-neuron input and output layer (identity activation, referred to as $id$). It has two hidden layers with four and two neurons, respectively, where neurons in the same layer may have different activation functions.

**Definition 2.** *Let* $C = \bigcup_{k=0}^{n} |\sigma_k|$ *where* $\sigma_k = \{v_0^k, v_1^k, \ldots, v_d^k\}$ *are the* $d$*-simplices of a* $d$*-dimensional simplicial complex* $K$*, and let* $g : \mathbb{R}^d \to \mathbb{R}$*. Then, for* $p \in \mathbb{R}^d$ *we define the global* BNN *as:*

$$\mathrm{BNN}(p) = \frac{1}{\#\{k : \mathrm{BNN}_{\sigma_k}\big((t_0^k, t_1^k, \ldots, t_d^k)\big) > 0\}} \cdot \sum_{k=0}^{n} \mathrm{BNN}_{\sigma_k}\big((t_0^k, t_1^k, \ldots, t_d^k)\big),$$

*where* $\#\{k : \mathrm{BNN}_{\sigma_k}\big((t_0^k, t_1^k, \ldots, t_d^k)\big) > 0\}$ *counts the number of local networks* $\mathrm{BNN}_{\sigma_k}$ *that are nonzero at the barycentric coordinates* $(t_0^k, t_1^k, \ldots, t_d^k)$ *of* $p$ *with respect to* $\sigma^k$*.*

In other words, the value of BNN at a point $p$ is the average of the values of the local networks $\mathrm{BNN}_{\sigma_k}$ for which $p$ lies in $|\sigma_k|$, which is precisely detected by $\mathrm{BNN}_{\sigma_k}\big((t_0^k, t_1^k, \ldots, t_d^k)\big) > 0$. This normalization properly accounts for overlapping simplices: points at the intersection of multiple simplices (e.g., shared vertices or edges) yield multiple nonzero local evaluations, and the BNN formula averages them to ensure continuity and consistency.

**Example 1.** *Suppose* $g : [A, B] \to \mathbb{R}$ *where* $\sigma_1 = \{a_1 = A, a_2 = b_1\}$ *and* $\sigma_2 = \{b_1 = a_2, b_2 = B\}$ *are two adjacent 1-simplices, we have that the barycentric coordinates of* $b_1 = a_2$ *with respect to* $\sigma_1$ *are* $(0, 1)$ *and with respect to* $\sigma_2$ *are* $(1, 0)$*. Then*

$$\begin{aligned}
\mathrm{BNN}_{\sigma_1}\big((0,1)\big) &= \mathrm{ReLU}\big(1 - \mathrm{ReLU}(1) - 2\cdot\mathrm{step}^*(0) - 2\cdot\mathrm{step}^*(-1)\big)\cdot g(a_1) \\
&\quad + \mathrm{ReLU}\big(1 - \mathrm{ReLU}(0) - 2\cdot\mathrm{step}^*(-1) - 2\cdot\mathrm{step}^*(0)\big)\cdot g(a_2) = g(a_2) \\
\mathrm{BNN}_{\sigma_2}\big((1,0)\big) &= \mathrm{ReLU}\big(1 - \mathrm{ReLU}(0) - 2\cdot\mathrm{step}^*(-1) - 2\cdot\mathrm{step}^*(0)\big)\cdot g(b_1) \\
&\quad + \mathrm{ReLU}\big(1 - \mathrm{ReLU}(1) - 2\cdot\mathrm{step}^*(0) - 2\cdot\mathrm{step}^*(-1)\big)\cdot g(b_2) = g(b_1).
\end{aligned}$$

*Then,* $\mathrm{BNN}_{\sigma_1}\big((0,1)\big)+\mathrm{BNN}_{\sigma_2}\big((1,0)\big)=g(a_2)+g(b_1)=2\cdot g(b_1)=2\cdot g(a_2)$ *(since* $b_1=a_2$*). This illustrates the redundancy at joining points and motivates the normalization in the global BNN.*

We present the following result, ensuring consistency, continuity and locality of BNNs.

**Theorem 4.1.** *Let* $C=\bigcup_{k=0}^{n}|\sigma_k|$ *where* $\sigma_k=\{v_0^k,v_1^k,\dots,v_d^k\}$ *are the* $d$*-simplices of a* $d$*-dimensional simplicial complex* $K$*, and let* $g:\mathbb{R}^d\to\mathbb{R}$*. We have:*

(1) $\mathrm{BNN}(v_\ell^k)=g(v_\ell^k)$ *for all* $\ell\in\{0,1,\dots,d\}$ *and* $k\in\{0,1,\dots,n\}$.

(2) *If* $p\in C$ *then*

$$\mathrm{BNN}(p)=\mathrm{BNN}_{\sigma^k}\big((t_0^k,t_1^k,\dots,t_d^k)\big)=\sum_{i=0}^{d}t_i^k\cdot g(v_i^k).$$

*where* $(t_0^k,t_1^k,\dots,t_d^k)$ *are the barycentric coordinates of* $p$ *with respect to* $\sigma_k$ *for any* $k$ *such that* $p\in|\sigma_k|$.

(3) *If* $p\notin C$ *then* $\mathrm{BNN}(p)=0$.

(4) *The function* $\mathrm{BNN}:C\to\mathbb{R}$ *is a CPLF.*

*Proof.* First, recall the definition of $\mathrm{BNN}_\sigma$ for a given point $p\in\mathbb{R}^d$ with barycentric coordinates $(t_0^k,t_1^k,\dots,t_d^k)$ with respect to a simplex $\sigma^k$:

$$\mathrm{BNN}_{\sigma_k}\big((t_0^k,t_1^k,\dots,t_d^k)\big)=\sum_{i=0}^{d}\mathrm{ReLU}\Big(1-\mathrm{ReLU}(1-t_i^k)-\sum_{j=0}^{d}\big(\mathrm{step}^*(-t_j^k)+\mathrm{step}^*(t_j^k-1)\big)\Big)\cdot g(v_i^k).$$

Now, let us prove the statements.

(1) By definition, the barycentric coordinates of $v_\ell^k$ with respect to $\sigma_k$ are $(0,\overset{\ell}{\dots},0,1,0\overset{d-\ell}{\dots},0)$ where the value 1 is at position $\ell$. Since $\mathrm{step}^*(0)=step^*(-1)=0$ and $1-\mathrm{ReLU}(1-0)=0$ then

$$\mathrm{BNN}_{\sigma_k}\big((0,\overset{\ell}{\dots},0,1,0\overset{d-\ell}{\dots},0)\big)=\mathrm{ReLU}\Big(1-\mathrm{ReLU}(1-1)\Big)\cdot g(v_\ell^k)=g(v_\ell^k).$$

Similarly, if $v_\ell^k=v_{\ell'}^{k'}$ for some $k'\in\{0,1,\dots,n\}$ and $\ell'\in\{0,1,\dots,d\}$ then

$$BNN_{\sigma_{k'}}\big((0,\overset{\ell'}{\dots},0,1,0\overset{d-\ell'}{\dots},0)\big)=g(v_{\ell'}^{k'})=g(v_\ell^k).$$

We can then conclude that, $\mathrm{BNN}(v_\ell^k)=g(v_\ell^k)$.

(2) If $p\in|\sigma_k|$ then by Lemma 1 we have that

$$\mathrm{BNN}_{\sigma_k}\big((t_0^k,t_1^k,\dots,t_d^k)\big)=\sum_{i=0}^{d}t_i^k\cdot g(v_i^k).$$

If $p\in|\sigma^i|\cap|\sigma^j|$ for some $i,j\in\{0,1,\dots,n\}$, let $(t_0^i,t_1^i,\dots,t_d^i)$ and $(t_0^j,t_1^j,\dots,t_d^j)$ be the barycentric coordinates of $p$ with respect to $\sigma_i$ and $\sigma_j$ respectively. By the definition of simplicial complexes, there is an $\ell$-simplex $\sigma=\{v_0,v_1,\dots,v_\ell\}\subset\sigma_i,\sigma_j$ with $\ell<d$ such that $p\in|\sigma|$ and satisfying that there are sets of indices $I,J\subset\{0,1,\dots,d\}$ such that $v_r=v_{r_i}^i=v_{r_j}^j$ and $t_r=t_{r_i}^i=t_{r_j}^j$ for some $r_i\in I$ and $r_j\in J$ and for all $r\in\{0,1,\dots,\ell\}$, being $(t_0,t_1,\dots,t_\ell)$ the barycentric coordinates of $p$ with respect to $\sigma$. Putting all together, we have that

$$\mathrm{BNN}_{\sigma^i}\big((t_0^i,t_1^i,\dots,t_d^i)\big)=\sum_{r_i\in I}t_{r_i}^i\cdot g(v_{r_i}^i)=\sum_{r_j\in I}t_{r_j}^j\cdot g(v_{r_j}^j)=BNN_{\sigma^j}\big((t_0^j,t_1^j,\dots,t_d^j)\big).$$

We then conclude that, for any $k\in\{0,1,\dots,n\}$ with $p\in|\sigma_k|$,

$$\mathrm{BNN}(p)=\sum_{i=0}^{d}t_i^k\cdot g(v_i^k)$$

where $(t_0^k,t_1^k,\dots,t_d^k)$ are the barycentric coordinates of $p$ with respect to $\sigma_k$.

(3) If $p \notin C$ then, $p \notin |\sigma_k|$ for any given $k \in \{0, 1, \ldots, n\}$. Therefore, by Lemma 1, $\mathrm{BNN}_{\sigma^k}\left((t_0^k, t_1^k, \ldots, t_d^k)\right) = 0$ and so $\mathrm{BNN}(p) = 0$.

(4) Let $p \in C$. Then $p \in |\sigma^k|$ for some $k \in \{0, 1, \ldots, n\}$. Let $(t_0^k, t_1^k, \ldots, t_d^k)$ be the barycentric coordinates of $p$ with respect to $\sigma_k$, by Lemma 1 and by the definition of barycentric coordinates, we have:

$$\begin{aligned}
\mathrm{BNN}(p) = \sum_{i=0}^{d} t_i^k \cdot g(v_i^k) &= \begin{pmatrix} g(v_0^k) & g(v_1^k) & \cdots & g(v_d^k) \end{pmatrix} \cdot \begin{pmatrix} t_0 & t_1 & \cdots & t_d \end{pmatrix}^T \\
&= \begin{pmatrix} g(v_0^k) & g(v_1^k) & \cdots & g(v_d^k) \end{pmatrix} \cdot \begin{pmatrix} v_0 & v_1 & \cdots & v_d \\ 1 & 1 & \cdots & 1 \end{pmatrix}^{-1} \cdot \begin{pmatrix} p \\ 1 \end{pmatrix} \\
&= \begin{pmatrix} m_0^k & m_1^k & \cdots & m_{d-1}^k & c_k \end{pmatrix} \cdot \begin{pmatrix} p \\ 1 \end{pmatrix} = m_k \cdot p + c_k
\end{aligned}$$

where $m_k \in \mathbb{R}^d$ and $c_k \in \mathbb{R}$, concluding the proof.

□

**Remark 5.** *Any* CPLF $g : [A, B] \to \mathbb{R}$ *can be represented by a* BNN*, with the key property that the* BNN *does not require an analytic definition. Instead, to specify the* CPLF *or the corresponding* BNN*, it is sufficient to provide a finite set of transition (base) points* $\{a_i\} \subset \mathbb{R}$*, where the* CPLF *shifts between linear segments, together with the* CPLF *value at these points. This allows the* BNN *to capture the contribution of each segment relative to the input, thereby generating the correct output. For consistency with the terminology introduced in the Introduction, in the following we shall refer to these transition points as* base points*.*

## 5 Testing BNNs and Length-Weighted Persistent Entropy-Based Loss in the Context of Resource-Efficient AI

In this section, we test the capabilities of our proposed framework under the context of *Resource-Efficient AI*, assuming that we have limited resources for network design and training, such as a small number of base points and few training epochs. Our approach combine BNN*s with a new topological loss function*, the length-weighted persistent entropy-based loss function, which, as its name suggests, is based on the persistent entropy variant proposed in Section 3, to approximate an objective function $f\colon [A, B] \to \mathbb{R}$, which is only known on a finite number of samples $S$, where $\{A, B\} \subset S \subset [A, B]$. A BNN is constructed from the limited set of base points, which define both its overall structure and its internal parameters. Consequently, BNNs are non-trainable in the conventional sense, meaning that training in our framework amounts to iteratively adjusting the base points, thereby shaping the architecture. To guide this optimisation, we propose using a topological loss based on our novel variant of persistent entropy, the *length-weighted persistent entropy* (LWPE), to guide the adjustment of base points and, consequently, the architecture of the BNNs, optimising their distribution and ensuring effective approximation. We present experiments that show how our topological loss can be used to optimize the distribution of the base points that define BNNs, approximating $f$ *better and faster* compared to using classical loss function, like mean squared error (MSE), root mean squared error (RMSE), mean absolute error (MAE), or the LogCosh. We used the Tensorflow[2] and Gudhi[3] libraries to implement our proposed BNN and our proposed topological loss, as well as to conduct our experiments.

First, we begin by noticing that a BNN, constructed using a set of equidistant base points, can effectively approximate any continuous nonlinear function $f : [A, B] \subset \mathbb{R} \to \mathbb{R}$, such as $f(x) = \sin(x)$. This relies on Remark 5, which states that any CPLF can be represented by a BNN, and Remark 1 that states that a CPLF, and therefore a BNN, acts as a universal approximator for continuous functions over compact intervals.

In more realistic scenarios, the resources available for network design and training are often limited. For instance, it may be unrealistic to employ as many as 150 base points. Instead, we consider a function $f : [A, B] \subset \mathbb{R} \to \mathbb{R}$ that is represented by a point cloud, defined as a set $X = \{(x_i, y_i)\}_{i \in I}$, where each pair $(x_i, y_i)$ is a sample point, that is, $y_i = f(x_i)$. In general, we say that a set $X$ is a *point-cloud-based function* if $x_i = x_j$ implies that $y_i = y_j$ for all $i, j \in I$. We aim to approximate $X$ using a BNN built from only a small, fixed number of base points, including the endpoints $A$ and $B$.

[2]The TensorFlow documentation is available at `https://www.tensorflow.org/`.

[3]The Gudhi documentation is available at `https://gudhi.inria.fr/`.

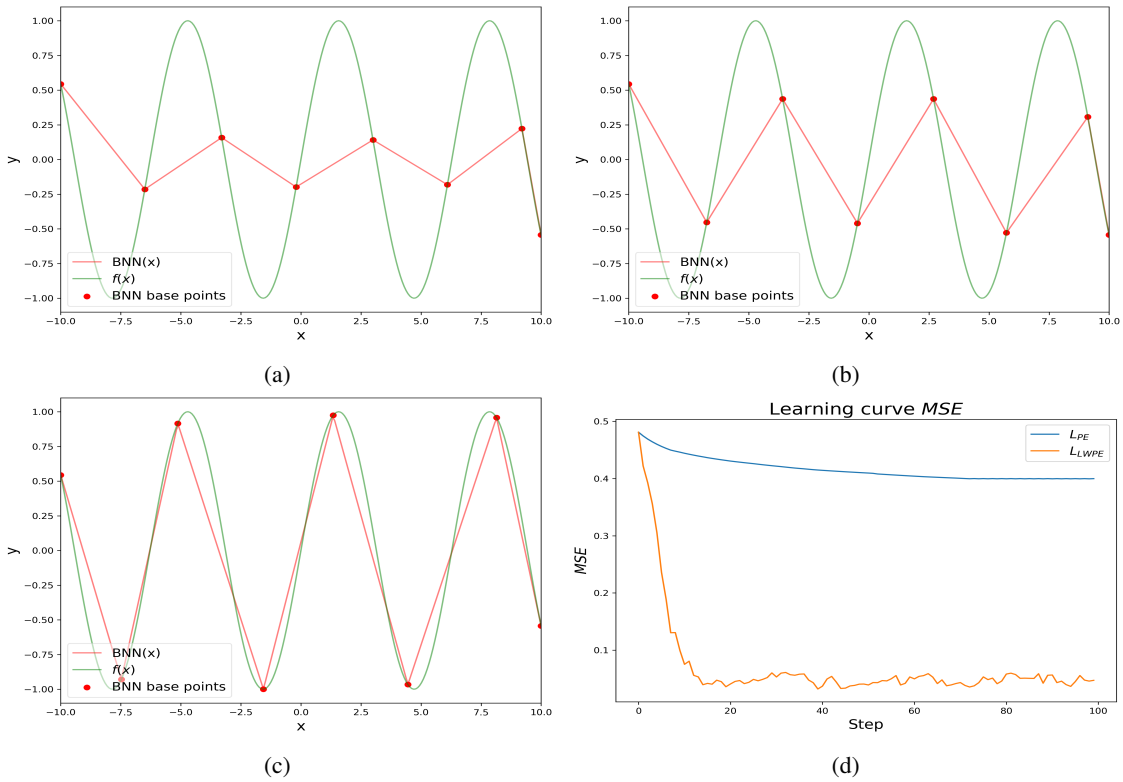


Figure 4: Comparison of function approximation using a BNN with 8 base points, optimized via two persistent entropy-based loss functions. (a) Initial state with randomly initialized base points. (b) Final iteration (50) using standard persistent entropy-based loss function ($L_{\mathrm{PE}}$). (c) Final iteration using our length-weighted persistent entropy-based loss function ($L_{\mathrm{LWPE}}$). (d) MSE learning curves showing convergence differences between $L_{\mathrm{PE}}$ and $L_{\mathrm{LWPE}}$.

Initially, we considered a topological loss function based on the standard persistent entropy:

$$L_{\mathrm{PE}} = |\,\mathrm{PE}_{\mathrm{ref}} - \mathrm{PE}_{\mathrm{pred}}\,| \tag{3}$$

where both $\mathrm{PE}_{\mathrm{ref}}$ and $\mathrm{PE}_{\mathrm{pred}}$ are the persistent entropy computed via the lower-star filtrations of the reference and predicted point clouds, respectively. The objective of this persistent entropy-based loss function is to minimize the absolute difference between the persistent entropy derived from the reference and predicted point cloud, ensuring a similar topological structure. However, this standard persistent entropy-based approach presents a fundamental limitation, as discussed in Section 3, since it does not necessarily guide the BNN and its base points towards an accurate pointwise approximation of the target function. This limitation is clearly shown in Fig 4, where, after optimizing the base points to approximate $f(x) = \sin(x)$ on the interval $[-10, 10]$ using $L_{\mathrm{PE}}$, the BNN converges to a representation that preserves the relative proportions of the peaks but fails to align with their true amplitudes and oscillatory structure. Consequently, even though the persistent entropy values of the reference and prediction remain close, the learned function does not capture the actual maxima and minima of the target.

To overcome this limitation, we employ our length-weighted persistent entropy (LWPE), introduced in Section 3, as the basis for the topological loss function, replacing the standard persistent entropy. As shown in Fig. 4, optimizing base points using LWPE for computing the loss function instead of PE yields a significantly closer fit to the target function. This observation is further supported by the learning curves in Fig.4d: while the standard entropy variant results to slower and limited convergence, our length-weighted version achieves rapid and stable minimization of the MSE, indicating more effective learning dynamics. Both experiments used SGD with a learning rate of 0.1 and limited resources: 50 epochs and 8 base points.

Consequently, we adopt $L_{\mathrm{LWPE}}$ as our default topological loss based on our proposed variant of persistent entropy throughout the remainder of the experiments. Formally, it is defined as:

$$L_{\mathrm{LWPE}} = |\,\mathrm{LWPE}_{\mathrm{ref}} - \mathrm{LWPE}_{\mathrm{pred}}\,|. \tag{4}$$

To test our framework's robustness, we evaluate its performance in approximating a noisy point cloud function using a limited and fixed number of base points. This scenario reflects more realistic applications, as in most real-world cases,

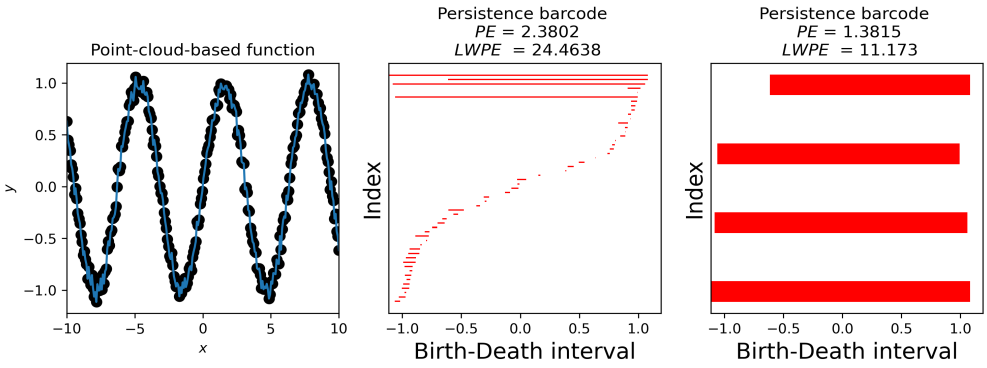


Figure 5: Similar point-cloud-based function consisting of 250 points as in Fig. 1, but with noise (left). The persistence barcode (middle) and its filtered version (right), showing only the 4 most significant bars, which illustrate the topological features that can be approximated using 8 base points to construct the BNN.

point clouds will not be as smooth as the one presented previously. A key constraint in this setup is that, with a fixed number of points $n$, we can at most approximate a function (sampled by a point cloud $X$) whose persistence barcode contains at most $n/2$ bars, or equivalently, the $n/2$ most significant bars, if we assume that the function contains noise. As an illustrative example, refer to Fig. 5, where we consider a point cloud $X$ with 250 points representing a partial description of the sine function with noise (left). As discussed above, and by analyzing the obtained barcode derived from $X$, we can deduce that with $n = 8$ points, we can at most approximate a function whose persistence barcode $D$ contains $n/2 = 4$ bars, or said in other words, we can approximate a barcode with the $n/2 = 4$ most longest bars of $D$ (considering the rest of the bars of $D$ as noise, as is represented in the right plot of Fig. 5).

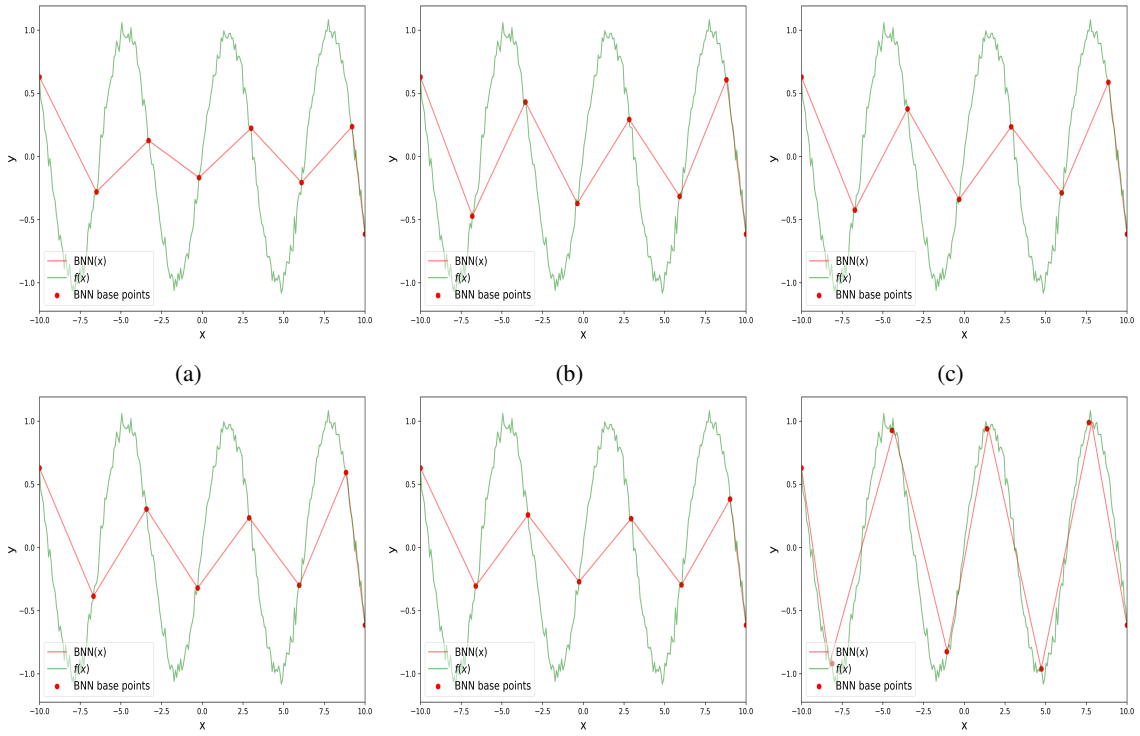


Figure 6: Approximation of a noisy point-cloud-based function using a BNN with 8 base points, optimized via different loss functions. (a) Initial state with randomly placed base points. (b–f) Final epoch (50) BNN approximation using the following losses: (b) MSE, (c) RMSE, (d) MAE, (e) LogCosh, (f) $L_{\text{LWPE}}$.

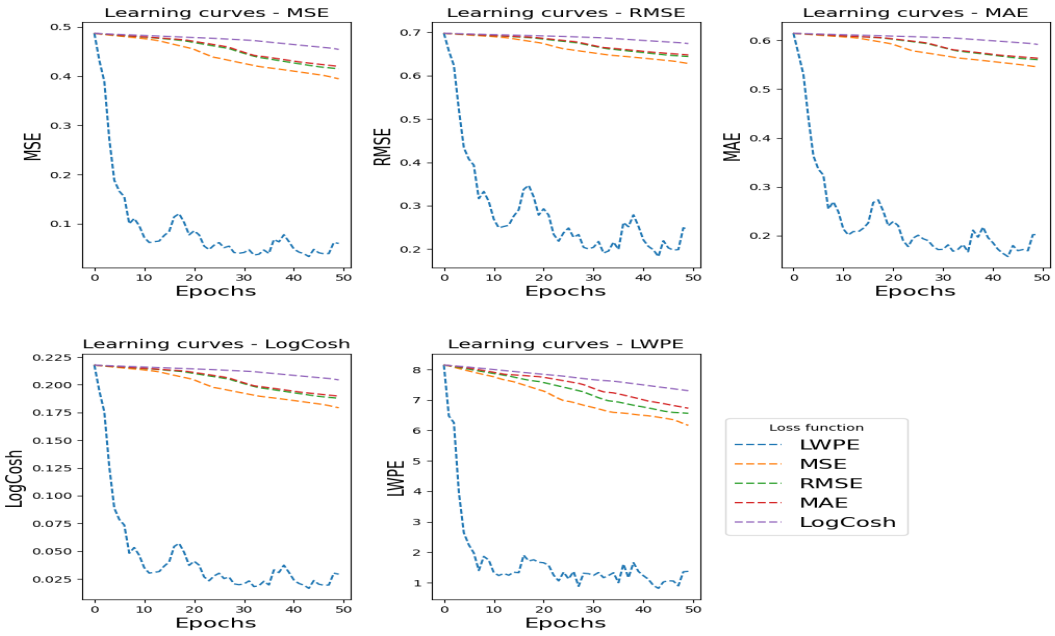


Figure 7: Learning curves for approximating a noisy point-cloud-based function using a BNN with 8 base points. The plots compare convergence across different loss functions used to optimize the base points: MSE, RMSE, MAE, LogCosh, and our length-weighted persistent entropy loss ($L_{\mathrm{LWPE}}$). Curves are ordered row-wise: first row, first column is MSE; first row, second column is RMSE; and so on.

In Fig. 6 we can see an example where we aim to approximate a noisy point cloud function, utilizing BNNs and our topological loss function $L_{\mathrm{LWPE}}$, as well as with more commonly used loss functions, such as MSE, RMSE, MAE, or the LogCosh, under limited resources (8 base points and 50 epochs). With $L_{\mathrm{LWPE}}$, the BNN achieves a more effective distribution of base points and, consequently, a superior approximation under the same constraints. Furthermore, the learning curves in Fig. 7 show that optimizing the base points with our topological loss function $L_{\mathrm{LWPE}}$ exhibits a superior and faster performance than using classical loss functions. This indicates that $L_{\mathrm{LWPE}}$ provides more informative gradients during the early training stages, enabling a quicker and more accurate optimization of base point distributions, and consequently, a better approximation, reinforcing our framework's effectiveness in handling complex and noisy data, even under limited settings.

To showcase the applicability of our method to real-world data, we approximate a financial time series: the daily price of a Gold ETF during the year 2023 (point-cloud-based function consisting of 365 points), obtained using the yfinance python library[4]. Having a limited number of 30 base points, we aim to capture the signal's essential structure, effectively treating this as a signal compression task that removes short-term noise. In Fig. 8, we observe that $L_{\mathrm{LWPE}}$ again outperforms the classical losses, reducing approximation error across all metrics within the first epochs, highlighting its suitability for approximation tasks and time-series compression with a limited number of base points and epochs.

In summary, using the $L_{\mathrm{LWPE}}$ to optimize the base points that define BNNs demonstrates clear benefits in approximating complex, noisy functions with very few base points and epochs. This makes it especially appealing for real-world applications having limited resources.

## 6 Conclusions

In this work, we introduced a novel framework for function approximation that integrates geometric modeling with topological optimization. Central to our approach is the Barycentric Neural Network (BNN), a shallow neural architecture whose structure and parameters are entirely determined by a fixed set of base points and their barycentric

[4]The yfinance documentation is available at `https://ranaroussi.github.io/yfinance/`

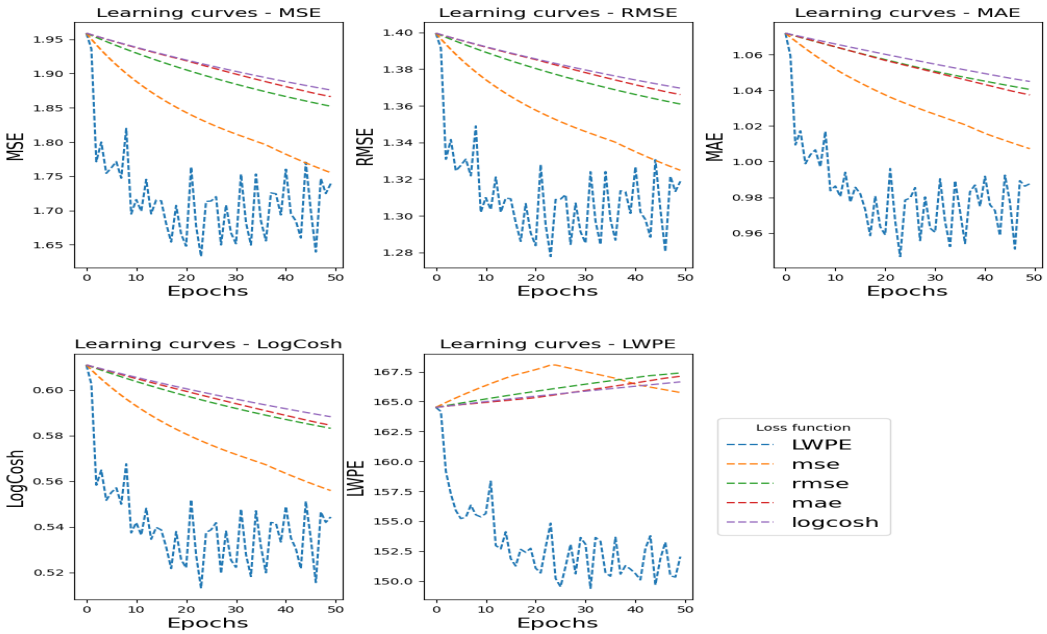


Figure 8: Learning curves for approximating gold ETF 2023 time series using a BNN with 30 base points. The plots compare convergence across different loss functions used to optimize the base points: MSE, RMSE, MAE, LogCosh, and our length-weighted persistent entropy loss ($L_{\mathrm{LWPE}}$). Curves are ordered row-wise: first row, first column is MSE; first row, second column is RMSE; and so on.

coordinates. This design enables exact representation of Continuous Piecewise Linear Functions (CPLFs) and allows the BNN to serve as a flexible, interpretable, and structurally predefined architecture (model) for approximating general continuous functions. Unlike traditional neural networks, which require optimization of internal weights through backpropagation, our BNN shifts the learning process to the optimization of the base point positions themselves. To guide this optimization, we proposed a novel loss function based on the length-weighted persistent entropy (LWPE). Our experimental results demonstrate that this BNN-LWPE framework achieves superior performance for function approximation compared to using classical loss functions (MSE, RMSE, MAE, and log-cosh), especially under resource-constrained settings, such as a limited and fixed number of points, and limited training epochs, making it a strong candidate for applications aligned with the principles of Green AI. Our method offers a mathematically principled and computationally efficient alternative to standard deep learning approaches for function approximation, contributing to the development of more interpretable, sustainable, and theoretically grounded machine learning models.

**Limitations** Despite its promising results, the proposed framework presents several limitations that merit discussion. A key challenge lies in the selection and initialization of the base points, which define the geometry of the BNN. Because the network's expressive power depends on these base points, poor initialization or insufficient point density can hinder convergence and compromise the quality of the approximation. The effectiveness of our topological loss is especially sensitive to the number and distribution of these points, which must be sufficient to capture the relevant information of the target function. Another limitation is linked to the nature of the function being approximated. Our topological loss is well-suited for functions with prominent and persistent topological structures, such as clear extrema or oscillatory behavior, but may underperform when applied to functions that are either highly irregular, noisy, or lack significant topological contrast. In such cases, the length-weighted persistent entropy-based loss function may fail to provide meaningful gradients, and statistical or hybrid loss functions might offer better alternatives. These limitations open avenues for future work on adaptive base point initialization strategies and hybrid loss functions that can combine topological and statistical information for more robust performance across a wider class of target functions.

**Future work** Future research focuses on extending this approach to higher-dimensional function approximation and exploring its applications in more real-world scenarios. In order to obtain the simplicial complex $\mathcal{K}$ that covers

a compact set $\mathcal{C} \subset \mathbb{R}^d$, we could, for example, compute Delaunay triangulations [11] with a set of vertices $V$ being a set of points of $\mathbb{R}^d$. Although the time complexity of such construction is roughly $O(n^{\lfloor d/2 \rfloor})$ (see [28]), it remains computationally feasible when $V$ is small enough. In addition, we aim to investigate adaptive initialization schemes for the base points, possibly incorporating prior information or combining topological and statistical heuristics. This would improve robustness and reduce the reliance on careful manual initialization. Furthermore, efforts will be directed toward formally proving the advantages of using our topological loss function. Additionally, the development of hybrid loss functions, which combine topological descriptors with classical metrics, may further enhance optimization in settings with noisy or weakly structured data. Another crucial direction is developing strategies to handle outliers in point-cloud-based function approximation, ensuring robustness against noisy data and improving generalization when dealing with real-world datasets.

**Code Availability** All code for the proposed methodology, as well as for generate the results presented in this manuscript, are publicly available in a Github repository [5].

**Disclosure of Interest** The authors have no competing interests to declare that are relevant to the content of this article.

## References


[1] Nieves Atienza, Rocio González-Diaz, and Manuel Soriano-Trigueros. On the stability of persistent entropy and new summary functions for topological data analysis. *Pattern Recognit.*, 107:107509, 2020.

[2] Helmut Bölcskei, Philipp Grohs, Gitta Kutyniok, and Philipp Petersen. Optimal approximation with sparsely connected deep neural networks. *SIAM J. Math. Data Sci.*, 1(1), 2019.

[3] Verónica Bolón-Canedo, Laura Morán-Fernández, Brais Cancela, and Amparo Alonso-Betanzos. A review of green artificial intelligence: Towards a more sustainable future. *Neurocomputing*, 599:128096, 2024.

[4] Mathieu Carrière, Marc Theveneau, and Théo Lacombe. Diffeomorphic interpolation for efficient persistence-based topological optimization. In *Proceedings of the 38th International Conference on Neural Information Processing Systems*, NIPS '24. Curran Associates Inc., 2025.

[5] Harish Chintakunta, Thanos Gentimis, Rocio Gonzalez-Diaz, Maria-Jose Jimenez, and Hamid Krim. An entropy-based persistence barcode. *Pattern Recognit.*, 48(2), 2015.

[6] David Cohen-Steiner, Herbert Edelsbrunner, and John Harer. Stability of persistence diagrams. *Discret. Comput. Geom.*, 37(1), 2007.

[7] Ana Dodik, Oded Stein, Vincent Sitzmann, and Justin Solomon. Variational barycentric coordinates. *ACM Trans. Graph.*, 42(6), December 2023.

[8] Herbert Edelsbrunner and J Harer. *Computational topology: an introduction*. AMS, 2022.

[9] Herbert Edelsbrunner and John Harer. Persistent homology—a survey. In *Surveys on Discrete and Computational Geometry: Twenty Years Later*, volume 453 of *Contemp. Math.*, pages 257–282. AMS, 2008.

[10] Silvia Ferrari and Robert F Stengel. Smooth function approximation using neural networks. *IEEE Trans. Neural Netw.*, 16(1), 2005.

[11] Steven Fortune. Voronoi diagrams and delaunay triangulations. In *Handbook of discrete and computational geometry*, pages 705–721. Chapman and Hall/CRC, 2017.

[12] Lee-Ad Gottlieb, Keran Kaufman, Aryeh Kontorovich, Gabriel Nivasch, and Ofir Pele. Nested barycentric coordinate system as an explicit feature map for polyhedra approximation and learning tasks. *Machine Learning*, 113, October 2024.

[13] Kevin Gurney. *An introduction to neural networks*. CRC press, 2018.

[14] Christoph Hofer, Roland Kwitt, Marc Niethammer, and Andreas Uhl. Deep learning with topological signatures. In *Proceedings of the 31st International Conference on Neural Information Processing Systems*, NIPS'17, page 1633–1643, Red Hook, NY, USA, 2017. Curran Associates Inc.

[15] Kurt Hornik, Maxwell Stinchcombe, and Halbert White. Multilayer feedforward networks are universal approximators. *Neural Netw.*, 2(5), 1989.


[5] `https://github.com/victosdur/Function_Approximation_Using_BNN_and_LWPE.git`

[16] Shiyu Liang and R. Srikant. Why deep neural networks for function approximation? In *Proc. of the 5th ICLR*, 2017.

[17] Zixin Lin, Nur Fariha Syaqina Zulkepli, Mohd Shareduwan Mohd Kasihmuddin, and R. U. Gobithaasan. Hybridizing persistent homology and machine learning for oceanographic time series. *Journal of Water and Climate Change*, 16(2), 2025.

[18] Bo Liu and Yi Liang. Optimal function approximation with relu neural networks. *Neurocomputing*, 435, 2021.

[19] Alexandra Malyugina, Nantheera Anantrasirichai, and David Bull. A topological loss function for image denoising on a new bvi-lowlight dataset. *Signal Processing*, 211:109081, 2023.

[20] James R. Munkres. *Topology*. Prentice Hall, 2nd edition, 2000.

[21] N. Otter, M.A. Porter, U. Tillmann, P. Grindrod, and H.A. Harrington. A roadmap for the computation of persistent homology. *EPJ Data Science*, 6(1):17, 2017.

[22] Eduardo Paluzo-Hidalgo, Rocio Gonzalez-Diaz, and Miguel A. Gutiérrez-Naranjo. Two-hidden-layer feed-forward networks are universal approximators: A constructive approach. *Neural Netw.*, 131, 2020.

[23] Philipp Petersen and Felix Voigtlaender. Optimal approximation of piecewise smooth functions using deep relu neural networks. *Neural Netw.*, 108:296–330, 2018.

[24] Ernst Röell and Bastian Rieck. Differentiable euler characteristic transforms for shape classification. In *International Conference on Learning Representations*, 2024.

[25] Matteo Rucco, Filippo Castiglione, Emanuela Merelli, and Marco Pettini. Characterisation of the idiotypic immune network through persistent entropy. In *Proc. of ECCS 2014*, 2016.

[26] Matteo Rucco, Rocio Gonzalez-Diaz, Maria-Jose Jimenez, Nieves Atienza, Cristina Cristalli, Enrico Concettoni, Andrea Ferrante, and Emanuela Merelli. A new topological entropy-based approach for measuring similarities among piecewise linear functions. *Signal Process.*, 134, 2017.

[27] Itay Safran and Ohad Shamir. Depth-width tradeoffs in approximating natural functions with neural networks. In *Proc. of the 34th ICML*, page 2979–2987. JMLR.org, 2017.

[28] R. Seidel. The upper bound theorem for polytopes: an easy proof of its asymptotic version. *Comput. Geom.*, 5(2), 1995.

[29] Victor Toscano-Duran, Sara Narteni, Alberto Carlevaro, Rocio Gonzalez-Diaz, Maurizio Mongelli, and Jerome Guzzi. Safe and efficient social navigation through explainable safety regions based on topological features, 2025.

[30] Joe Warren, Scott Schaefer, Anil N Hirani, and Mathieu Desbrun. Barycentric coordinates for convex sets. *Adv. Comput. Math.*, 27, 2007.

[31] Zarita Zainuddin and Ong Pauline. Function approximation using artificial neural networks. *WSEAS Trans. Math.*, 7(6):333–338, 2008.

[32] Yikai Zhang, Jiachen Yao, Yusu Wang, and Chao Chen. On the convergence of optimizing persistent-homology-based losses, 2022.

[33] Ali Zia, Abdelwahed Khamis, James Nichols, Usmun Bashir Tayab, Zeeshan Hayder, Vivien Rolland, Eric Stone, and Lars Petersson. Topological deep learning: a review of an emerging paradigm. *Artificial Intelligence Review*, 57, 2024.